
Facilitate Collaboration between Large Language Model and Task-specific Model for Time Series Anomaly Detection

Feiyi Chen¹ Leilei Zhang² Guansong Pang³ Roger Zimmermann⁴ Shuiguang Deng¹

Abstract

In anomaly detection, methods based on large language models (LLMs) can incorporate expert knowledge, while task-specific smaller models excel at extracting normal patterns and detecting value fluctuations. Inspired by the human nervous system—where the brain stores expert knowledge and the peripheral nervous system and spinal cord handle specific tasks like withdrawal and knee-jerk reflexes—we propose CoLLaTe, a framework designed to facilitate collaboration between LLMs and task-specific models, leveraging the strengths of both. In this work, we first formulate the collaboration process and identify two key challenges in the collaboration between LLMs and task-specific models: (1) the misalignment between the expression domains of LLMs and smaller models, and (2) error accumulation arising from the predictions of both models. To address these challenges, we introduce two key components in CoLLaTe: the alignment module and the collaborative loss function. Through theoretical analysis and experimental validation, we demonstrate that these components effectively mitigate the identified challenges and achieve better performance than LLM based methods and task-specific smaller model.

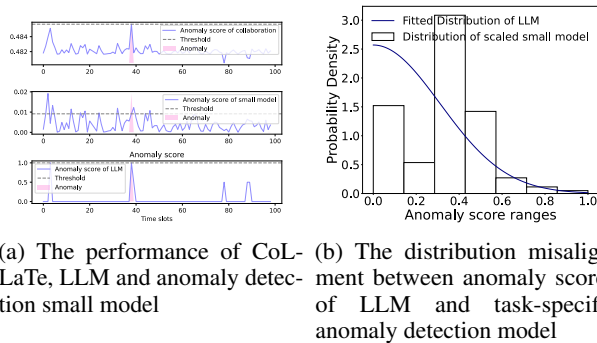
1. Introduction

Recently, methods based on Large Language Models (LLMs) have demonstrated strong generalization capabilities, effectively leveraging human expertise to complete

a wide range of tasks. However, they are often insensitive to the value fluctuations in time series data, and their NLP-based representations do not align well with the characteristics of time series data (Jin et al., 2024). In contrast, task-specific methods, such as anomaly detection models, typically lack the broad generalization capabilities of LLMs across multiple tasks. However, these models are specifically designed for particular tasks and often exhibit superior performance when applied to well-matched anomaly detection datasets (Zhou et al., 2023). Despite their strengths, task-specific models also have notable limitations. First, for different application scenarios, researchers need to adapt anomaly detection models to incorporate domain-specific expertise to achieve optimal performance. For instance, anomaly detection methods tailored for cloud service monitoring (Ma et al., 2021; Chen et al., 2024b) or aircraft monitoring (e Silva & Murcca, 2023) have been modified to suit these specific contexts. Second, in many practical scenarios, such as aircraft monitoring (Nanduri & Sherry, 2016), it is not feasible to collect data for all possible flight conditions. These conditions often represent distinct distributions and normal patterns in the monitoring data. This lack of comprehensive data coverage significantly hinders the performance of task-specific anomaly detection models.

Inspired by the human nervous system—which relies on the brain to store expert knowledge and extract general principles, while using the peripheral nervous system and spinal cord for specific tasks like the withdrawal reflex and knee-jerk reflex—we propose a framework called CoLLaTe. This framework facilitates the **Collaboration** between a **Large Language** model (LLM, analogous to the brain) and a **Task-specific** model (analogous to the peripheral nervous system and spinal cord). CoLLaTe leverages the complementary strengths of both LLMs and task-specific anomaly detection methods. By enabling collaboration between an LLM and a task-specific anomaly detection model, we can integrate domain expertise from various application scenarios into the task-specific model without making any adaptation to the model. This approach also mitigates performance degradation caused by insufficient monitoring data across diverse operational conditions, because LLMs excel at utilizing professional documents to incorporate domain knowledge, which is often expressed in natural language.

¹Department of Computer Science and Technology, Zhejiang University, Zhejiang, China ²Company Name, Location, Country ³Singapore Management University ⁴National University of Singapore, Department of Computer Science and Technology, Singapore. Correspondence to: Shuiguang Deng <dengsg@zju.edu.cn>, Leilei Zhang <xxx@xxx.edu.cn>.



(a) The performance of CoLLaTe, LLM and anomaly detection small model

(b) The distribution misalignment between anomaly scores of LLM and task-specific anomaly detection model

Figure 1. (a) The figure shows the anomaly score of LLM, anomaly detection small model and CoLLaTe respectively. (b) The figure shows the anomaly score histogram of task-specific small model for anomaly detection and the fitted curve of anomaly score of LLM on Mustang.

Such knowledge is highly condensed and can cover more general situations compared to concrete data samples. For instance, comparing with giving different time series and telling whether they are trigonometric or not, giving the rule $a \sin(w_1 x + t_1) + b \cos(w_2 x + t_2)$ is more condensed and can represent more general situations. Thus, in cases where training data samples are scarce, LLMs can extract general standards from professional documents to guide anomaly detection and mitigate the performance degradation due to data shortage.

CoLLaTe integrates an LLM, enhanced by professional documents, with a task-specific anomaly detection model to assess the severity of anomalies for each time slot. Subsequently, CoLLaTe employs a conditional network to combine the judgments from the LLM and the anomaly detection model, using the data representation from the small model as a condition, to produce a unified anomaly score. As illustrated in Fig. 1(a), the collated anomaly score retains the true positive judgments from both the LLM and the small model while reconciling false positives. During this collaborative process, two main challenges arise:

- Misalignment between the expression domains of the LLM and the task-specific model: The LLM and the task-specific model interpret anomaly scores differently, meaning they may use the same score to represent different levels of anomaly severity. For example, as shown in Fig. 1(b), most anomaly scores produced by the LLM are below 0.3, whereas the anomaly scores generated by the small model are predominantly centered around 0.4. Consequently, an anomaly score of 0.4 might indicate a moderate anomaly for the LLM, but for the small model, it could signify a normal condition. Such inconsistencies in score interpretation can disrupt effective collaboration between the two models.

- Error Accumulation: Both the LLM and the task-specific anomaly detection model are subject to prediction errors. During the collaboration process, these errors may not cancel out but instead accumulate. Through mathematical analysis and experimental validation, we demonstrate that when employing classical loss functions, such as Mean Squared Error (MSE), the errors from the small model and the LLM tend to compound rather than offset.

To enable effective collaboration between the LLM and the task-specific anomaly detection model while addressing the challenges mentioned above, we have made the following key contributions:

- We first formalize the collaboration process between the LLM and the task-specific model, identifying the key challenges that arise during this process. To address these challenges, we propose a framework that facilitates seamless collaboration between the LLM and the task-specific model.
- We introduce a novel alignment module to harmonize the differing interpretations of anomaly scores between the LLM and the task-specific anomaly detection model.
- We conduct a theoretical analysis of the error accumulation phenomenon that occurs during the collaboration process and propose a novel loss function to mitigate it. Furthermore, we theoretically demonstrate several fascinating properties of the optimal solution to the proposed loss function and experimentally validate its effectiveness.
- We conducted extensive experiments to validate the effectiveness of CoLLaTe and each of its proposed modules.

2. Preliminary

Given a task-specific small model and a LLM, they gives an anomaly score and a representation to each time slot of a time series X , as shown in Eq. 1-Eq. 2, where \hat{s} and S are anomaly scores given by different models respectively and R is the representation of time slots. X_i is the i^{th} time slot of X . \hat{s}_i and S_i are anomaly score of i^{th} time slot respectively. y_i is 1 when X_i is anomalous. Otherwise, it is 0. CoLLaTe uses the representation R as condition to synthesize the anomaly score of small model and the one of LLM, as shown in Eq. 3. CoLLaTe makes collated anomaly score \hat{S} approach y unsupervisedly and overpasses the performance of task-specific small model and LLM.

$$\hat{s}, R = \text{SmallModel}(X) \quad (1)$$

$$S = \text{LLM}(X) \quad (2)$$

$$\hat{S} = \text{CoLLaTe}(\hat{s}, S; R) \quad (3)$$

3. Method

3.1. Overview

The architecture of CoLLaTe is shown in Fig. 2. The anomaly scores \hat{s} and S are obtained from a task-specific small model and a LLM respectively, where the LLM uses a set-up pitch prompt illustrated in subsection. 3.2. Anomaly scores \hat{s} and S usually have different understandings of anomaly scores, i.e. LLM and task-specific model can use same score to denote different anomalous degrees. Thus, we propose an Alignment module to align the different understandings of LLM and task-specific model for same anomaly scores. After that, we use a conditional network to synthesize aligned scores of task-specific model and LLM with the representation as condition. In this way, we obtain the collated anomaly score \hat{S} . Furthermore, we propose a collaborative loss function, which can effectively leverage the compensative effect between LLM and task-specific small model and LLM. Besides, it is proven it can avoid error accumulation during the collaborative process of task-specific small model and LLM.

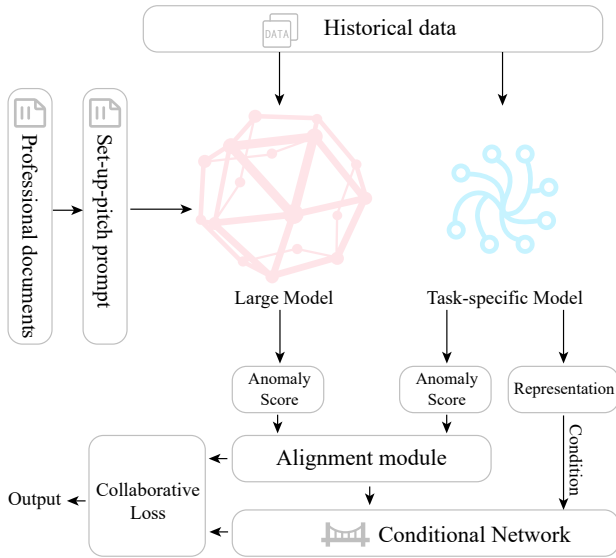


Figure 2. The model architecture of CoLLaTe

3.2. Set-up-pitch Prompt

There are many works prove that invoking similar historical examples in prompt can significantly improve the anomaly detection performance (Liu et al., 2024b). Thus, our prompt consisted of four parts: the expertise supplementation, task description, input data, examples. The expertise supple-

mentation section encompasses the specific meanings of different dimensions of input data within the application domain, as well as the relevant professional expertise, such as value ranges and the relationships between different dimensions. The task description section instruct the large language model to judge whether the given time slot is anomalous and stipulate the output formation. The example section contains a positive and a negative example. We list the concrete prompt in appendix A.5. Recent works invoke examples from a fixed dataset. However, the normal pattern always varies as time pass by in many application scenarios. For example, in cloud server monitoring, the cloud environment always changes from time to time as the services update, deployment and revocation (Chen et al., 2024a; Ma et al., 2021). In aircraft monitoring, the normal patterns change as the condition of flight and aircraft changes. As shown in Fig. 3(a), we made an experiment on our aircraft monitoring data, which prove that the longer time distance between the given time slot for anomaly detection and time slot of example, the worse the performance of GPT4 is. Therefore, with the assistance of a small task-specific model for anomaly detection, we regularly update the collection of examples.

3.3. Alignment Module

Task-specific small model and LLM usually have different understanding of anomaly score, i.e. they use same anomaly score to denote different serious degree of anomalies. There are two factors contribute to this problem: the value range and distribution misalignment. Most of reconstruction-based small models use reconstruction error as the anomaly score, which makes the range of anomaly score various. However, the anomaly score of LLM is constrained to $[0, 1]$. The huge gap between the anomaly score ranges of LLM and task-specific small model will cause different understanding of anomaly scores and degrade the collaboration performance. To solve this problem we firstly scale anomaly score of small model by Eq. 4, where d is a hyperparameter, \hat{s}_{max} and \hat{s}_{min} are the maximum and minimum values of small model anomaly scores.

$$s = \frac{\hat{s}}{\sqrt{d(\hat{s}_{max} - \hat{s}_{min})}} \quad (4)$$

Even if scaled anomaly scores of small model, different anomaly score distribution will cause different understanding of anomaly scores. As shown in Fig. 3(b), we use a half-gaussian distribution, which will be elaborated in the following, to fit the histogram of LLM anomaly scores. Then, we shift the fitted curve to the histogram of task-specific small model anomaly score in Fig. 1(b), where we can find that most anomaly scores are under 0.3 for LLM, while the anomaly scores of small model centered at $[0.3, 0.4]$. Thus, the anomaly score of 0.4 may mean moderate anomaly risks for LLM, while it may only mean normal for

the small model. In this situation, if we directly let the small model and LLM to collaborate without alignment, it may distort the original purpose of each model (i.e. LLM scores a time slot as 0.4, small model deem this as LLM thinks the time slot is normal). Thus, we propose alignment module to deal with this challenge.

Inspired by the teaching manage rules in Universities, which stipulates the proportion of each score level to align the scores given by different professors (e.g. control the pass rate and excellence rate), we design the alignment module to align the distributions of anomaly scores of LLM and task-specific small model, so that the same anomaly score of LLM and small model can denote similar anomalous degree. We first use half-Gaussian distribution to fit the distribution $f(S)$ of LLM. The half-Gaussian distribution is shown in Eq. 5. We fit it by obtaining the negative mirror image set of the initial anomaly scores and then merge it with the original set and estimating the standard variance of the new set as the σ in Eq. 5.

$$f(S) = \begin{cases} \frac{2}{\sigma\sqrt{2\pi}}e^{-\frac{S^2}{2\sigma^2}}, & S \geq 0 \\ 0, & S < 0 \end{cases} \quad (5)$$

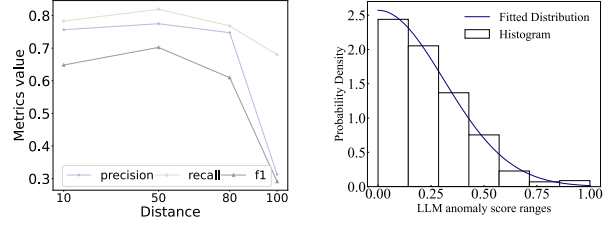
Subsequently, we use a mapping function $\mathcal{M}(s)$ to map $s \in \{s_i\}_{i=0}^n$ to a new set, whose distribution should approach $f(S)$. To achieve this, we divide the value range of anomaly scores, $[0, 1]$, into N bins. We use c_i to denote how many mapped scores $\mathcal{M}(s)$ fall into the i^{th} bin. Then, we minimize cross entropy to decrease the distance between $f(S)$ and the distribution mapped set as Eq. 6 shows, where $\hat{\mu}, \hat{\sigma}$ are the mean and standard variance of distribution $f(S)$ and $\mu_M = \frac{1}{n} \sum_{k=1}^n \mathcal{M}(s_k)$. The problem of Eq. 6 is that the counting process of c_i is non-differentiable and could not be used in backward propagation.

$$\begin{aligned} \min. & - \sum_{i=1}^N \frac{c_i}{\sum_{j=1}^N c_j} \log \left[\int_{(i-1)/N}^{i/N} f(S) dS \right] \\ \text{s.t.} & \frac{1}{n} \sum_{k=1}^n \mathcal{M}(s_k) = \hat{\mu} \\ & \frac{1}{n-1} \sum_{k=1}^n [\mathcal{M}(s_k) - \mu_M]^2 = \hat{\sigma}^2 \end{aligned} \quad (6)$$

To solve above problem, we propose Theorem 1 and we uses Eq. 7 as our loss function instead.

Theorem 1. When N approach infinite, Eq. 6 can be transformed to Eq. 7, which is differentiable. $\hat{\lambda}_1$ and $\hat{\lambda}_2$ are hyperparameters.

The proof of Theorem 1 is given in Appendix. A.1.



(a) The performance of GPT4 for different distances from example (b) Anomaly score distribution for different distances from example

Figure 3. (a) The figure shows the anomaly detection performance of GPT4 when the distance between designated time slot for anomaly detection and the time slot of example. (b) The figure shows the histogram of anomaly score of LLM on Mustang (Amvrosiadis et al., 2018) dataset and the fitted curve of the anomaly score.

Table 1. The average F1 score of task-specific small model and GPT4 on plane monitoring dataset.

	Contextual	Point
Small model	0.561	0.061
GPT4	0.409	0.231

$$\begin{aligned} \mathcal{L}_a = & - \frac{1}{n} \sum_{i=1}^n \log(f(\mathcal{M}(s_i))) + \hat{\lambda}_1 \left(\frac{1}{n} \sum_{i=1}^n \mathcal{M}(s_i) - \hat{\mu} \right)^2 \\ & + \hat{\lambda}_2 \left(\frac{1}{n-1} \sum_{i=1}^n (\mathcal{M}(s_i) - \mu_M)^2 - \hat{\sigma}^2 \right)^2 \end{aligned} \quad (7)$$

3.4. Collaborative Loss

Many anomaly detection works divides anomalies into contextual anomaly and point anomaly (Schmidl et al., 2022; Tuli et al., 2022). We made experiments on 4 plane monitoring datasets, which are described in Appendix. A.7. The results in Tab. 1 demonstrated the compensative performance of task-specific small model and LLM on contextual anomaly and point anomaly, where F1 score of contextual anomaly for small model is better than the one of GPT4, while F1 score of point anomaly for GPT4 is better than the one of small model. Thus, we introduce a conditional network, which uses the representation R of input data obtained by small model as the condition, the aligned anomaly score of small model and LLM as input and output a collated anomaly score, as show in Eq. 8, where \mathcal{P} is the trainable parameter of the conditional network.

$$\hat{S} = \text{ConditionalNet}(\mathcal{M}(s), S, R; \mathcal{P}) \quad (8)$$

To leverage the compensative performance of small model

and GPT4, we design a loss function to adaptively adjust the collated anomaly score. We firstly divide the time series into patches (Nie et al., 2023). For each time slot we compute the average distance between present time slot with other time slots in same patch and denote it by D_{intra} . Then, we compute the average distance between the patch of present time slot and other patches and denote it by D_{inter} . The bigger difference between D_{intra} and D_{inter} is, the more likely that the present time slot is a point anomaly and LLM can judge it more accurate and vice versa. Thus, we design the loss function as in Eq.9, where $\mathcal{L}(a, b)$ represent a loss function measuring the distance between a and b .

$$\mathcal{L}_b = \frac{D_{intra}}{D_{intra} + D_{inter}} \mathcal{L}(s, \hat{S}) + \frac{D_{inter}}{D_{intra} + D_{inter}} \mathcal{L}(S, \hat{S}) \quad (9)$$

If we choose some popular loss function formation, such as $\mathcal{L}(a, b) = (a - b)^2$, it will accumulate the prediction error of small model and LLM in the process of gradient descent, as show in Theorem 2, which is proven in Appendix. A.2.

Assumption 1. The anomaly score prediction error of task specific small model is ϵ_s , where ϵ_s obeys an unknown distribution $\mathcal{D}_s(\mu_s, \sigma_s)$, $\mu_s \neq 0$.

Assumption 2. The anomaly score prediction error of LLM is ϵ_S , where ϵ_S is the LLM prediction error, which obeys an unknown distribution $\mathcal{D}_S(\mu_S, \sigma_S)$, $\mu_S \neq 0$.

Assumption 3. \mathcal{L}'_b is L -Lipschitz continuous.

Theorem 2. Given Assumption 1 - Assumption 2, when $\mathcal{L}(a, b) = (a - b)^2$, the difference between optimal solution \hat{S}^* of \mathcal{L}_b and ground truth $y = \mathbb{E}[(\hat{S}^* - y)^2] \geq (\lambda_1 \mu_s + \lambda_2 \mu_S)^2$, where $\lambda_1 = \frac{D_{intra}}{D_{intra} + D_{inter}}$ and $\lambda_2 = \frac{D_{inter}}{D_{intra} + D_{inter}}$.

From Theorem 2, we can find that when using MSE as \mathcal{L} , the expectation prediction error of conditional network is greater than the weighted sum of the expectation of small model prediction error and the one of LLM, which denotes the error accumulation between small model and LLM. This phenomenon is also observed in experiment and discussed in subsection. 4.4.

To solve this problem we propose collaborative loss function as show in Eq. 10, where \hat{S}_i , s_i and S_i are anomaly scores of i^{th} sample output by conditional network, small model and LLM respectively. In Lemma 1, we prove that using the collaborative loss function is approximate to using loss function in Eq. 11, which proves that Eq. 10 avoid error of small model and LLM to accumulate, since Eq. 11 directly let the difference between collated anomaly scores of two samples approach the ground truth. We also experimentally prove Eq. 10 can avoid error accumulation and discuss it in subsection. 4.4. Furthermore, in Theorem 3, we prove the optimal solution of Eq. 10 has two properties. The property 1 denotes that if the anomaly degree of time slot r is more serious than the on of time slot k , the optimal

collated anomaly score of time slot r is bigger than the one of time slot k . The property 2 denotes that if the difference of anomaly degree between time slot r and time slot k is bigger than the one between time slot r' and time slot k' , the difference of optimal collated anomaly scores can also reflect this gap.

$$\mathcal{L}_b = -\frac{1}{n^2} \sum_{i=1}^n \sum_{j=1}^n \lambda_1 [(s_i - s_j)(\hat{S}_i - \hat{S}_j)] + \lambda_2 [(S_i - S_j)(\hat{S}_i - \hat{S}_j)] \quad (10)$$

Lemma 1. When Assumption 1 - Assumption 3 hold, as the iteration steps T approach infinity, minimizing Eq. 10 by stochastic gradient descent can be approximate to minimizing Eq. 11 by stochastic gradient descent with convergence rate $\mathcal{O}(T^{-\frac{1}{4}})$.

$$\mathcal{L}'_b = -\sum_{i=1}^n \sum_{j=1}^n [(y_i - y_j)(\hat{S}_i - \hat{S}_j)] \quad (11)$$

The proof of Lemma 1 is given in Appendix. A.3.

Theorem 3. When Assumption 1 - Assumption 3 hold, the optimal solution \hat{S}^* of the loss function in Eq. 10 satisfies following properties.

Property 1. $\forall r, \forall k$, if the ground truth $y_r > y_k$, then $\hat{S}_r^* > \hat{S}_k^*$, where y_r and y_k denotes the ground truth of anomaly score of r^{th} and k^{th} sample respectively, \hat{S}_r^* and \hat{S}_k^* are the ground truth of anomaly score of r^{th} and k^{th} sample respectively.

Property 2. $\forall r, \forall k, \forall r', \forall k'$, if the ground truth $y_r - y_k > y_{r'} - y_{k'}$, then $\hat{S}_r^* - \hat{S}_k^* > \hat{S}_{r'}^* - \hat{S}_{k'}^*$.

The proof of Theorem 3 is given in Appendix. A.4.

3.5. Train and Inference

During the training process, we use $\mathcal{L}_a + \mathcal{L}_b$ as the loss function. During the inference process, we use the collated anomaly score output by conditional network as the anomaly score and use POT algorithm to determine the threshold (Siffer et al., 2017). When anomaly score is higher than the threshold, the time slot is judged as anomaly.

4. Experiment

We have made extensive experiments to on four datasets and make following contributions:

- CoLLaTe can achieve the best performance compared with SOTA LLM-based anomaly detection methods and small-model-based anomaly detection methods.
- We locate the hyperparameters that are important to CoLLaTe performance and analyze their effect.

Table 2. The average performance of CoLLaTe and baselines on four datasets.

	Mustang			MGAB			Flight1			Flight2		
	Prec	Rec	F1	Prec	Rec	F1	Prec	Rec	F1	Prec	Rec	F1
GPT4	0.586	0.797	0.552	0.813	0.970	0.862	0.754	0.673	0.620	0.322	1.000	0.422
LLMAD	0.068	0.800	0.122	0.077	0.696	0.132	0.138	<u>0.982</u>	0.226	0.171	0.873	0.274
sigLLM	-	-	-	0.063	0.589	0.107	-	-	-	-	-	-
MSCRED	0.871	0.960	0.896	0.829	0.960	0.882	0.690	0.947	<u>0.768</u>	0.502	0.987	0.595
OmniAnom	0.812	<u>0.968</u>	0.878	0.761	0.995	0.822	0.619	1.000	0.721	0.579	1.000	0.637
TranAD	0.865	0.918	0.867	0.301	0.500	0.367	0.340	1.000	0.497	0.225	1.000	0.367
AnomalyTr	1.000	0.891	<u>0.935</u>	<u>0.934</u>	0.807	0.851	0.750	0.649	0.685	0.549	0.469	0.484
DCdetector	<u>0.968</u>	0.718	0.799	0.200	0.200	0.200	<u>0.759</u>	0.615	0.664	0.749	0.742	<u>0.746</u>
CoLLaTe [†]	0.914	1.000	0.953	0.927	0.996	<u>0.959</u>	0.606	1.000	0.729	<u>0.682</u>	0.762	0.627
CoLLaTe [‡]	0.615	0.933	0.738	0.490	0.996	0.578	0.675	0.830	0.667	0.416	0.991	0.529
CoLLaTe [*]	0.968	0.933	0.943	0.522	0.970	0.594	0.631	0.894	0.648	0.436	0.755	0.530
CoLLaTe [*]	0.950	0.933	0.931	0.925	0.996	<u>0.957</u>	0.566	1.000	0.694	<u>0.775</u>	0.819	0.702
CoLLaTe	0.950	1.000	0.971	0.970	0.996	0.982	0.790	0.978	0.866	0.897	0.891	0.883

- All the modules in CoLLaTe are effective and contribute to its performance.
- We further explore and analyze the compensative effect between LLM and task-specific small model.

4.1. Experiment Setup

Baselines. We compare CoLLaTe with SOTA anomaly detection methods: DCdetector (Yang et al., 2023), AnomalyTransformer (Xu et al., 2022), TranAD (Tuli et al., 2022), OmniAnomaly (Su et al., 2019), MSCRED (Zhang et al., 2019). Besides, we also introduce SOTA LLM-based anomaly detection methods: GPT4, LLMAD (Liu et al., 2024b), sigLLM (Alnegheimish et al., 2024). Besides, we use CoLLaTe[†], CoLLaTe[‡], CoLLaTe^{*} to denote CoLLaTe removing alignment module, changing collaborative loss to MSE, changing $\frac{D_{inter}}{D_{inter}+D_{intra}}$ and $\frac{D_{intra}}{D_{inter}+D_{intra}}$ to 1. We use CoLLaTe^{*} to denote CoLLaTe removing LLM and conditional network.

Datasets. We choose one Cloud service monitoring dataset (Amvrosiadis et al., 2018), two plane monitoring datasets we collected from an airline company that belongs to one of the world’s top 150 enterprises. Besides, we also choose mathematical-assumption-based anomaly detection MGAB (Thill et al., 2020). Please refer to Appendix. A.7 for more details.

Hyperparameters. We show the values of hyperparameter in Appendix A.8.

Evaluation Metrics. We use three of most popular evaluation metrics to measure the performance of CoLLaTe, as many works did (Chen et al., 2022b; 2021; Li et al., 2023): the recall, precision and F1 score.

4.2. Prediction Accuracy

The four datasets used in our experiment all contain many subsets. We take 40% of each subset as the training set, 10% as the validate set, and the remaining 50% as the testing set. We compute precision, recall and F1 score for each subset, compute the average results and show them in Tab. 2, where we use "prec" and "rec" to denote precision and recall, and use "OmniAnom" and "AnomalyTr" for "OmniAnomaly" and "AnomalyTransformer". Since sigLLM is designed for univariate time series and can not apply to datasets Mustang Flight 1 and Flight 2, we do not list its performance on these datasets. As shown in Tab. 2, CoLLaTe can achieve best F1 score across four datasets. In Tab. 2, GPT4 is the LLM method used set-up-pitch prompt, which is exactly the LLM part of CoLLaTe. By comparing the performance of GPT4 and some other LLM-based anomaly detection methods, such as sigLLM and LLMAD, we can find that set-up-pitch prompt can greatly improve the anomaly detection accuracy of LLM. In Fig. 4(a), we use the precision and recall of best F1 score as the coordinates and draw the performance distribution of CoLLaTe, GPT4 and CoLLaTe^{*}, from which we can find that LLM and task-specific small model (CoLLaTe^{*}) either has poor precision or poor recall and CoLLaTe can achieve good performance on both metrics. This observation verifies that CoLLaTe can let task-specific small model and LLM collaborate with each other effectively and achieve better performance.

4.3. Hyperparameter Sensitivity

We explore the impact of d in Eq. 4, patch size for D_{inter} and D_{intra} , learning rate, $\hat{\lambda}_1$ and $\hat{\lambda}_2$ in Eq. 7 on the performance of CoLLaTe. When $\hat{\lambda}_1$ and $\hat{\lambda}_2$ change from $[0.01, 0.9]$, the change of F1 score of CoLLaTe is within 0.01. Thus, we mainly analyze the impact of d , patch size and learning rate. In Fig. 4(b), we test the F1 score of CoL-

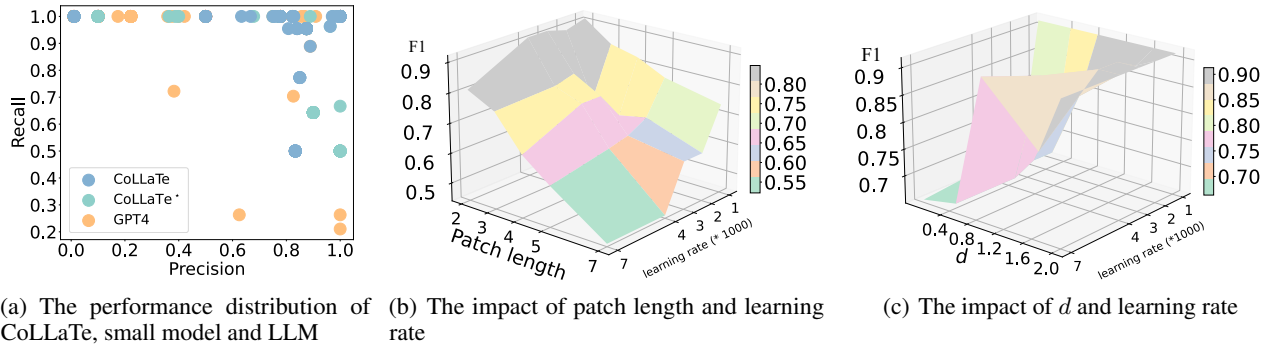


Figure 4. (a) The figure shows changes in F1 score as patch length in D_{inter} , D_{intra} and learning rate vary, where the learning rate ticks are the original value multiplied by 1000 times; (b) The figure shows changes in F1 score as d and learning rate vary, where the learning rate ticks are the original value multiplied by 1000 times; (c) We use a coordinates (Precision, Recall) to denote performance on a subset of flight dataset. We draw a scatter plot to show the distribution of LLM (GPT4), task-specific small model (CoLLaTe*) and CoLLaTe.

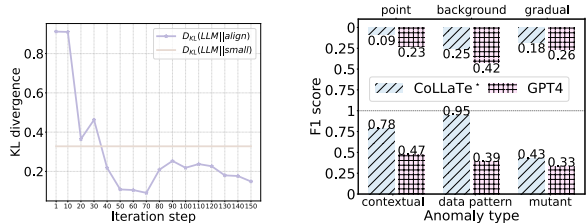


Figure 5. (a) The figure shows that KL-divergence between the histogram of LLM anomaly score and aligned small model anomaly score decrease as iteration step grows and compare the KL-divergence between LLM anomaly score and original small model anomaly score with the KL-divergence between LLM anomaly score and aligned small model anomaly score; (b) The figure shows the F1 score of LLM (GPT4) and task-specific small model (CoLLaTe*) when using different anomaly binary classification criteria.

LaTe when patch size of D_{inter} and D_{intra} changes from 2 to 7 and learning rate changes from 0.001 to 0.007. As Fig. 4(b) shows, the F1 score increases as learning rate and patch size get smaller. CoLLaTe can get better performance when patch size get smaller, because if patch size is much bigger than the length of contextual anomaly, D_{inter} will also be small. In this situation, since for both contextual anomaly and point anomaly D_{inter} is small and D_{intra} is big, the contextual anomaly and point anomaly can not be distinguished. This will degrade the performance of CoLLaTe. In Fig. 4(c), we test the F1 score of CoLLaTe when d changes from 0.01 to 2 and learning rate changes from 0.001 to 0.007. As Fig. 4(c) shows, the F1 score of CoLLaTe increases as d grows up. The performance of CoLLaTe also become more stable to learning rate as d grows up. Besides, smaller learning rate can usually make CoLLaTe work better when d is in the range of $[0.01, 2]$.

4.4. Effectiveness of Each Module

Ablation experiment. In CoLLaTe[†], we remove align module. In CoLLaTe[‡], we change $\mathcal{L}(a, b)$ to MSE. In CoLLaTe*, we change $\frac{D_{intra}}{D_{inter}+D_{intra}}$ and $\frac{D_{inter}}{D_{inter}+D_{intra}}$ to 1. We compare their performance with CoLLaTe in Tab. 2, where CoLLaTe outperform all of them. This proves that each module in CoLLaTe contributes to its performance.

Effectiveness of Collaborative Loss. CoLLaTe* is the small model used in CoLLaTe. By comparing the performance of CoLLaTe, GPT4 and CoLLaTe*, by collaborating small model CoLLaTe* and LLM-based model GPT4, CoLLaTe can work better than both of them, which verifies CoLLaTe effectively avoid error accumulation in the process of collaborating GPT4 and CoLLaTe*.

Effective of the design of $\mathcal{L}(a, b)$. Moreover, as mentioned above, CoLLaTe[‡] is the method that changes $\mathcal{L}(a, b)$ in collaborative loss function to MSE. On dataset MGAB, the performance of CoLLaTe[‡] is even worse than both

of GPT4 and CoLLaTe* and on other datasets, the performance of CoLLaTe[‡] are always worse than one of GPT4 and CoLLaTe* and slightly better than another. This observation verifies the analysis in subsection 3.4 that when using MSE as the formation of \mathcal{L}_b , the error of LLM and task-specific small model will accumulate during the process of collaboration.

Effectiveness of adaptive hyperparameters. In CoLLaTe*, we change the adaptive hyperparameters $\frac{D_{intra}}{D_{inter}+D_{intra}}$ and $\frac{D_{inter}}{D_{inter}+D_{intra}}$ to 1. By comparing it to GPT4 and the small model CoLLaTe*, we can find that on most datasets (MGAB, Flight 1, Flight 2), after changing the adaptive hyperparameters to 1, the performance of CoLLaTe* is between the performance of the LLM (GPT4) and task-specific small model (CoLLaTe*). That is because without effectively utilizing the compensative effect between LLM and task-specific small model, after collaborating, the performance of CoLLaTe* is only a compromise between the one with better performance and the one with lower performance. This observation prove the effectiveness of adaptive hyperparameters.

Effectiveness of Alignment module. The ablation experiment of CoLLaTe[†] can prove that alignment module can contribute to the performance of CoLLaTe. To verify that align module can effectively reduce the distribution distance between aligned anomaly score of task-specific small model and anomaly score of LLM. In Fig. 5(a), we show the KL-divergence distance between the original anomaly score histogram of small model and the one of LLM. Besides, we also show the variation of KL-divergence between aligned anomaly score histogram of small model and the anomaly score histogram of LLM as iteration step grows up. From Fig. 5(a), we can find that the distribution distance between aligned anomaly score and anomaly score of LLM gradually decreases as iteration step grows up and finally decreases to below the distribution distance between original small model anomaly score and the one of LLM, which verifies that align module can align the distribution of small model anomaly score and the one of LLM.

4.5. Compensative Effect

In CoLLaTe, we mainly utilize the the performance difference of LLM and task-specific small model on point anomaly and contextual anomaly. Actually, there are other compensative effect between small model and LLM by using other binary classification standard, and we explore them in this subsection. We introduce two kinds of binary classification standard: the anomalies needed expertise knowledge to detect and the anomalies can be detected only by data pattern, the gradual anomalies and mutual anomalies. These anomalies are illustrated in detail in Appendix. A.6. We divide Flight 2 in pieces and gather the pieces only obtain only

one kind of anomalies. We test GPT4 and CoLLaTe* on them and compute their average F1 score, which is shown in Fig. 5(b). In Fig. 5(b), we can see that LLM always has better performance on one kind of anomalies and has poorer performance on another in each binary anomaly classification.

5. Related work

Anomaly detection methods roughly fall into two streams: the classical anomaly detection methods and neural network based methods. The classical anomaly detection methods mainly utilize statistical model (Eskin, 2000; Wang et al., 2016), linear model (Ma & Perkins, 2003; Amer et al., 2013; Hu et al., 2003), and proximity analysis (Li et al., 2021; Izakian & Pedrycz, 2014) to figure out anomalies. The statistical models formulate the distribution of time series and judge anomalies based on the probability of each time series according to the fitted distribution. These methods rely on specific assumptions that limit their robustness in detecting anomalies in highly dynamic application scenarios (Ma et al., 2021). The linear-model-based methods transform the original time series to other space and figure out the boundaries between anomalies and normalities. The proximity-analysis-based methods using clustering models to classify anomalies and normalities. These methods do not consider the temporal dependency in time series and could not figure out contextual anomalies that violates temporal dependency (Wang et al., 2024). The neural-network-based methods can be divided into prediction-based methods (Malhotra et al., 2015; Hundman et al., 2018; Zong et al., 2018; Chen et al., 2022a), reconstruction-based methods (Chen et al., 2022b; You et al., 2022; Jiang et al., 2022; Shen et al., 2021; Tian et al., 2019) and LLM-based methods (Liu et al., 2024b; Russell-Gilbert et al., 2024; Liu et al., 2024a). The prediction-based methods detect anomalies by comparing the difference between prediction value and the ground truth. However, these methods are vulnerable to the historical inference (Wang et al., 2024). The reconstruction based methods can conquer this deficiency and show strong advantages over other methods, but they can not utilize expert knowledge in application scenario without model adaptation. Besides, they distinguish anomalies by learning the normal patterns from training data and pick data samples different from learned patterns as anomalies. However, in the application scenarios, where we can not observe and collect all the normal patterns of the anomaly detection objective, such as airplane monitoring, reconstruction-based methods can not work. In contrast, LLM based methods can effectively introduce the expertise knowledge by retrieval-augmented generation (RAG) (Lewis et al., 2020) and chain of thought (COT) (Wei et al., 2022), which do not require model modification. However, as a natural-language-based model, LLM is insensitive to value fluctuation and normal

pattern extraction. Moreover, the representation mismatch between natural language and time series also hinder the performance of LLM (Jin et al., 2024). None of these methods can utilize both the strengths of LLM based methods and task-specific small models. Thus, we propose CoLLaTe to improve anomaly detection performance.

6. Conclusion

Considering the compensative effect between LLM and task-specific small model, where LLM are more generalizable and can effectively embed expertise knowledge without model modification, and task-specific small model is more sensitive to value fluctuation and normal pattern extraction, we firstly formulate the collaboration process between LLM and task-specific, inspired by human nervous system. We firstly identify the collaboration challenges and propose a collaborative framework, called CoLLaTe to solve them. We have made solid mathematical proof and extensive experiments to verify the effectiveness of proposed methods.

References

- Alnegheimish, S., Nguyen, L., Berti-Equille, L., and Veeramachaneni, K. Large language models can be zero-shot anomaly detectors for time series? *arXiv preprint arXiv:2405.14755*, 2024.
- Amer, M., Goldstein, M., and Abdennadher, S. Enhancing one-class support vector machines for unsupervised anomaly detection. In *Proceedings of the ACM SIGKDD workshop on outlier detection and description*, pp. 8–15, 2013.
- Amvrosiadis, G., Park, J. W., Ganger, G. R., Gibson, G. A., Baseman, E., and DeBardleben, N. On the diversity of cluster workloads and its impact on research results. In *2018 USENIX Annual Technical Conference (USENIX ATC 18)*, pp. 533–546, 2018.
- Boyd, S. and Vandenberghe, L. *Convex optimization*. Cambridge university press, 2004.
- Bu, Z., Wang, Y.-X., Zha, S., and Karypis, G. Automatic clipping: Differentially private deep learning made easier and stronger. *Advances in Neural Information Processing Systems*, 36, 2024.
- Chen, C., Xie, Y., Lin, S., Yao, A., Jiang, G., Zhang, W., Qu, Y., Qiao, R., Ren, B., and Ma, L. Comprehensive regularization in a bi-directional predictive network for video anomaly detection. In *Proceedings of the AAAI Conference on Artificial Intelligence*, volume 36, pp. 230–238, 2022a.
- Chen, F., Qin, Z., Zhou, M., Zhang, Y., Deng, S., Fan, L., Pang, G., and Wen, Q. Lara: A light and anti-overfitting retraining approach for unsupervised time series anomaly detection. In *Proceedings of the ACM on Web Conference 2024*, pp. 4138–4149, 2024a.
- Chen, F., Zhang, Y., Fan, L., Liang, Y., Pang, G., Wen, Q., and Deng, S. Cluster-wide task slowdown detection in cloud system. In *Proceedings of the 30th ACM SIGKDD Conference on Knowledge Discovery and Data Mining*, pp. 266–277, 2024b.
- Chen, W., Tian, L., Chen, B., Dai, L., Duan, Z., and Zhou, M. Deep variational graph convolutional recurrent network for multivariate time series anomaly detection. In *International Conference on Machine Learning, ICML 2022*, volume 162 of *Proceedings of Machine Learning Research*, pp. 3621–3633, 2022b.
- Chen, X., Deng, L., Huang, F., Zhang, C., Zhang, Z., Zhao, Y., and Zheng, K. Daemon: Unsupervised anomaly detection and interpretation for multivariate time series. In *2021 IEEE 37th International Conference on Data Engineering (ICDE)*, pp. 2225–2230. IEEE, 2021.
- e Silva, L. C. and Murcca, M. C. R. A data analytics framework for anomaly detection in flight operations. *Journal of Air Transport Management*, 110:102409, 2023.
- Eskin, E. Anomaly detection over noisy data using learned probability distributions. 2000.
- Hu, W., Liao, Y., and Vemuri, V. R. Robust anomaly detection using support vector machines. In *Proceedings of the international conference on machine learning*, volume 6. Citeseer University Park, PA, USA, 2003.
- Hundman, K., Constantinou, V., Laporte, C., Colwell, I., and Soderstrom, T. Detecting spacecraft anomalies using lstms and nonparametric dynamic thresholding. In *Proceedings of the 24th ACM SIGKDD international conference on knowledge discovery & data mining*, pp. 387–395, 2018.
- Izakian, H. and Pedrycz, W. Anomaly detection and characterization in spatial time series data: A cluster-centric approach. *IEEE Transactions on Fuzzy Systems*, 22(6): 1612–1624, 2014.
- Jiang, X., Liu, J., Wang, J., Nie, Q., Wu, K., Liu, Y., Wang, C., and Zheng, F. Softpatch: Unsupervised anomaly detection with noisy data. *Advances in Neural Information Processing Systems*, 35:15433–15445, 2022.
- Jin, M., Wang, S., Ma, L., Chu, Z., Zhang, J. Y., Shi, X., Chen, P., Liang, Y., Li, Y., Pan, S., and Wen, Q. Time-llm: Time series forecasting by reprogramming large language models. In *The Twelfth International Conference on Learning Representations, ICLR 2024, Vienna, Austria, May 7-11, 2024*, 2024.

- Lai, C.-Y. A., Sun, F.-K., Gao, Z., Lang, J. H., and Boning, D. Nominality score conditioned time series anomaly detection by point/sequential reconstruction. *Advances in Neural Information Processing Systems*, 36, 2024.
- Lewis, P., Perez, E., Piktus, A., Petroni, F., Karpukhin, V., Goyal, N., Küttler, H., Lewis, M., Yih, W.-t., Rocktäschel, T., et al. Retrieval-augmented generation for knowledge-intensive nlp tasks. *Advances in Neural Information Processing Systems*, 33:9459–9474, 2020.
- Li, J., Izakian, H., Pedrycz, W., and Jamal, I. Clustering-based anomaly detection in multivariate time series data. *Applied Soft Computing*, 100:106919, 2021.
- Li, Y., Chen, W., Chen, B., Wang, D., Tian, L., and Zhou, M. Prototype-oriented unsupervised anomaly detection for multivariate time series. In *International Conference on Machine Learning, ICML 2023*, volume 202 of *Proceedings of Machine Learning Research*, pp. 19407–19424, 2023.
- Liu, C., He, S., Zhou, Q., Li, S., and Meng, W. Large language model guided knowledge distillation for time series anomaly detection. *arXiv preprint arXiv:2401.15123*, 2024a.
- Liu, J., Zhang, C., Qian, J., Ma, M., Qin, S., Bansal, C., Lin, Q., Rajmohan, S., and Zhang, D. Large language models can deliver accurate and interpretable time series anomaly detection. *arXiv preprint arXiv:2405.15370*, 2024b.
- Ma, J. and Perkins, S. Time-series novelty detection using one-class support vector machines. In *Proceedings of the International Joint Conference on Neural Networks, 2003.*, volume 3, pp. 1741–1745. IEEE, 2003.
- Ma, M., Zhang, S., Chen, J., Xu, J., Li, H., Lin, Y., Nie, X., Zhou, B., Wang, Y., and Pei, D. Jump-starting multivariate time series anomaly detection for online service systems. In *2021 USENIX Annual Technical Conference (USENIX ATC 21)*, pp. 413–426, 2021.
- Malhotra, P., Vig, L., Shroff, G., Agarwal, P., et al. Long short term memory networks for anomaly detection in time series. In *Esann*, volume 2015, pp. 89, 2015.
- Nanduri, A. and Sherry, L. Anomaly detection in aircraft data using recurrent neural networks (rnn). In *2016 Integrated Communications Navigation and Surveillance (ICNS)*, pp. 5C2–1. Ieee, 2016.
- Nie, Y., Nguyen, N. H., Sinthong, P., and Kalagnanam, J. A time series is worth 64 words: Long-term forecasting with transformers. In *The Eleventh International Conference on Learning Representations, ICLR 2023, Kigali, Rwanda, May 1-5, 2023*. OpenReview.net, 2023. URL <https://openreview.net/forum?id=Jbdc0vTOcol>.
- Osder, S. Practical view of redundancy management application and theory. *Journal of Guidance, Control, and Dynamics*, 22(1):12–21, 1999.
- Rakelly, K., Shelhamer, E., Darrell, T., Efros, A. A., and Levine, S. Conditional networks for few-shot semantic segmentation. In *6th International Conference on Learning Representations, ICLR 2018, Vancouver, BC, Canada, April 30 - May 3, 2018, Workshop Track Proceedings*, 2018.
- Russell-Gilbert, A., Sommers, A., Thompson, A., Cummins, L., Mittal, S., Rahimi, S., Seale, M., Jaboure, J., Arnold, T., and Church, J. Aad-llm: Adaptive anomaly detection using large language models. *arXiv preprint arXiv:2411.00914*, 2024.
- Schmidl, S., Wenig, P., and Papenbrock, T. Anomaly detection in time series: a comprehensive evaluation. *Proceedings of the VLDB Endowment*, 15(9):1779–1797, 2022.
- Shen, L., Yu, Z., Ma, Q., and Kwok, J. T. Time series anomaly detection with multiresolution ensemble decoding. In *Proceedings of the AAAI Conference on Artificial Intelligence*, volume 35, pp. 9567–9575, 2021.
- Siffer, A., Fouque, P.-A., Termier, A., and Largouet, C. Anomaly detection in streams with extreme value theory. In *Proceedings of the 23rd ACM SIGKDD international conference on knowledge discovery and data mining*, pp. 1067–1075, 2017.
- Su, Y., Zhao, Y., Niu, C., Liu, R., Sun, W., and Pei, D. Robust anomaly detection for multivariate time series through stochastic recurrent neural network. In *Proceedings of the 25th ACM SIGKDD international conference on knowledge discovery & data mining*, pp. 2828–2837, 2019.
- Thill, M., Konen, W., and Bäck, T. Time series encodings with temporal convolutional networks. In *International Conference on Bioinspired Methods and Their Applications*, pp. 161–173. Springer, 2020.
- Tian, K., Zhou, S., Fan, J., and Guan, J. Learning competitive and discriminative reconstructions for anomaly detection. In *Proceedings of the AAAI Conference on Artificial Intelligence*, volume 33, pp. 5167–5174, 2019.
- Tuli, S., Casale, G., and Jennings, N. R. TranAD: Deep transformer networks for anomaly detection in multivariate time series data. *Proc. VLDB Endow.*, 15(6):1201–1214, 2022.
- Wang, C., Zhuang, Z., Qi, Q., Wang, J., Wang, X., Sun, H., and Liao, J. Drift doesn't matter: dynamic decomposition with diffusion reconstruction for unstable multivariate time series anomaly detection. *Advances in Neural Information Processing Systems*, 36, 2024.

- Wang, W., Zhang, B., Wang, D., Jiang, Y., Qin, S., and Xue, L. Anomaly detection based on probability density function with kullback–leibler divergence. *Signal Processing*, 126:12–17, 2016.
- Wei, J., Wang, X., Schuurmans, D., Bosma, M., Xia, F., Chi, E., Le, Q. V., Zhou, D., et al. Chain-of-thought prompting elicits reasoning in large language models. *Advances in neural information processing systems*, 35:24824–24837, 2022.
- Xu, J., Wu, H., Wang, J., and Long, M. Anomaly transformer: Time series anomaly detection with association discrepancy. In *The Tenth International Conference on Learning Representations, ICLR 2022*. OpenReview.net, 2022.
- Yang, Y., Zhang, C., Zhou, T., Wen, Q., and Sun, L. Dcdetector: Dual attention contrastive representation learning for time series anomaly detection. In *Proceedings of the 29th ACM SIGKDD Conference on Knowledge Discovery and Data Mining, KDD 2023*, pp. 3033–3045. ACM, 2023.
- You, Z., Cui, L., Shen, Y., Yang, K., Lu, X., Zheng, Y., and Le, X. A unified model for multi-class anomaly detection. *Advances in Neural Information Processing Systems*, 35: 4571–4584, 2022.
- Zhang, C., Song, D., Chen, Y., Feng, X., Lumezanu, C., Cheng, W., Ni, J., Zong, B., Chen, H., and Chawla, N. V. A deep neural network for unsupervised anomaly detection and diagnosis in multivariate time series data. In *Proceedings of the AAAI conference on artificial intelligence*, volume 33, pp. 1409–1416, 2019.
- Zhou, T., Niu, P., Sun, L., Jin, R., et al. One fits all: Power general time series analysis by pretrained lm. *Advances in neural information processing systems*, 36:43322–43355, 2023.
- Zong, B., Song, Q., Min, M. R., Cheng, W., Lumezanu, C., Cho, D., and Chen, H. Deep autoencoding gaussian mixture model for unsupervised anomaly detection. In *6th International Conference on Learning Representations, ICLR 2018*, 2018.

A. Appendix

A.1. Proof of Theorem 1

$$\begin{aligned}
 \min . & - \sum_{i=1}^N \frac{c_i}{\sum_{j=1}^N c_j} \log \left[\int_{(i-1)b/N}^{ib/N} f(S) dS \right] \\
 \text{s.t.} & \quad \frac{1}{n} \sum_{k=1}^n \mathcal{M}(s_k) = \hat{\mu} \\
 & \quad \frac{1}{n-1} \sum_{k=1}^n [\mathcal{M}(s_k) - \mu_M]^2 = \hat{\sigma}^2
 \end{aligned} \tag{12}$$

In this part, we prove formation in Eq. 12 can be transformed to Eq. 14, when let N approach infinite. When N approach infinite, the optimization objective in Eq. 12 can be transformed to $\min . \lim_{N \rightarrow \infty} - \sum_{i=1}^N \frac{c_i}{\sum_{j=1}^N c_j} \log f(\frac{ib}{N})$. For each c_i , there will be two situations. One is that there is no $\mathcal{M}(s_j) = \frac{ib}{N}, j \in [1, n]$, then $c_i = 0$ and the item including c_i can be omitted. Another one is that there are some $\mathcal{M}(s_j) = \frac{ib}{N}, j \in [1, n]$, then c_i is equal to the number of times that $\frac{ib}{N}$ appears in $\{\mathcal{M}(s_j) | s_j \in \{s_j\}_{j=1}^n\}$. In this situation, the original item $\frac{c_i}{\sum_{j=1}^N c_j} \log f(\frac{ib}{N})$ can be transformed to $\frac{c_i}{n} \log f(\mathcal{M}(s_j))$, since $\sum_{j=1}^N c_j = n$. We cluster the mapping scores with a same value as a group, from which we can obtain M groups with values of $\{\mathcal{M}(s_{\hat{j}})\}_{\hat{j}=1}^M$. The size of \hat{j}^{th} group is exactly c_i , where $ib/N = \mathcal{M}(s_{\hat{j}})$. We denote the c_i as $c_{\hat{j}}$. The $\{c_{\hat{j}}\}_{\hat{j}=1}^M$ consist of the non-zero part of $\{c_i\}_{i=1}^N$. Then the original formation can be transformed to $\min . - \sum_{\hat{j}=1}^M \frac{c_{\hat{j}}}{n} \log f(\mathcal{M}(s_{\hat{j}}))$, which is exactly equal to traversing all the $\mathcal{M}(s_i), s_i \in \{s_i\}_{i=1}^n$, sum them up as $\sum_{i=1}^n \log(f(\mathcal{M}(s_i)))$, and combine the items with same value of mapping scores.

$$\begin{aligned}
 \min . & - \frac{1}{n} \sum_{i=1}^n \log(f(\mathcal{M}(s_i))) \\
 \text{s.t.} & \quad \frac{1}{n} \sum_{k=1}^n \mathcal{M}(s_k) = \hat{\mu} \\
 & \quad \frac{1}{n-1} \sum_{k=1}^n [\mathcal{M}(s_k) - \mu_M]^2 = \hat{\sigma}^2
 \end{aligned} \tag{13}$$

Then, we obtain Eq. 13. After that, by using Lagrange Multiplier method, we can transform Eq. 13 to Eq. 14, where $\hat{\lambda}_1 > 0, \hat{\lambda}_2 > 0$.

$$\begin{aligned}
 \min . & - \frac{1}{n} \sum_{i=1}^n \log(f(\mathcal{M}(s_i))) + \hat{\lambda}_1 \left(\frac{1}{n} \sum_{i=1}^n \mathcal{M}(s_i) - \hat{\mu} \right)^2 \\
 & + \hat{\lambda}_2 \left(\frac{1}{n-1} \sum_{i=1}^n (\mathcal{M}(s_i) - \mu_M)^2 - \hat{\sigma}^2 \right)^2
 \end{aligned} \tag{14}$$

A.2. Proof of Theorem 2

When $\mathcal{L}(a, b) = (a-b)^2$, we can transform Eq. 9 to Eq. 15, where $\lambda_1 = \frac{D_{intra}}{D_{intra} + D_{inter}}$ and $\lambda_2 = \frac{D_{inter}}{D_{intra} + D_{inter}}$. According to KKT condition (Boyd & Vandenberghe, 2004), the optimal solution of \mathcal{L}_b should satisfy Eq. 16. As shown in Appendix A.9, the gradient of architecture of conditional network can not be equal to 0. Thus, $2\lambda_1(y + \epsilon_s - \hat{S}^*(\mathcal{P}) + 2\lambda_2(y + \epsilon_S - \hat{S}^*(\mathcal{P}))) = 0$. Then, $\hat{S}^*(\mathcal{P}) = y + \lambda_1 \epsilon_s + \lambda_2 \epsilon_S$. Thus, $\mathbb{E}[(\hat{S}^*(\mathcal{P}) - y)^2] = \mathbb{E}[(\lambda_1 \epsilon_s + \lambda_2 \epsilon_S)^2]$. Since $f(x) = x^2$ is a convex function, according to Jensen's Inequality, $\mathbb{E}[(\lambda_1 \epsilon_s + \lambda_2 \epsilon_S)^2] \geq [\mathbb{E}(\lambda_1 \epsilon_s + \lambda_2 \epsilon_S)]^2$. Since $\epsilon_1 \sim \mathcal{D}_f(\mu_s, \sigma_s), \epsilon_2 \sim \mathcal{D}_S(\mu_S, \sigma_S)$,

$[\mathbb{E}(\lambda_1 \epsilon_s + \lambda_2 \epsilon_S)]^2 = (\lambda_1 \mu_1 + \lambda_2 \mu_2)^2$. Thus, $\mathbb{E}[(\hat{S}^*(\mathcal{P}) - y)^2] \geq (\lambda_1 \mu_1 + \lambda_2 \mu_2)^2$

$$\lambda_1(y + \epsilon_s - \hat{S}(\mathcal{P}))^2 + \lambda_2(y + \epsilon_S - \hat{S}(\mathcal{P}))^2 \quad (15)$$

$$2\lambda_1(y + \epsilon_s - \hat{S}^*(\mathcal{P})) \frac{\partial \hat{S}^*(\mathcal{P})}{\partial \mathcal{P}} + 2\lambda_2(y + \epsilon_S - \hat{S}^*(\mathcal{P})) \frac{\partial \hat{S}^*(\mathcal{P})}{\partial \mathcal{P}} = 0 \quad (16)$$

A.3. Proof of Lemma 1

When using stochastic gradient descent algorithm, the gradient of Eq. 9 and Eq. 11 is shown in Eq. 17 and Eq. 18 respectively, where \mathcal{B} is the set of sample in batch and $|\mathcal{B}|$ is the size of set $\{(r, t) | r \in \mathcal{B}, t \in \mathcal{B}\}$. Let $\mathbf{g}'_{i,j}$ denote the item in Eq. 18, whose index is (i, j) . Let $\mathbf{g}_{i,j}$ denote the item in Eq. 17, whose index is (i, j) . $\mathbf{g}_{i,j}$ can be transformed to $\mathbf{g}'_{i,j} + [\lambda_1(\epsilon_{s,i} - \epsilon_{s,j}) + \lambda_2(\epsilon_{S,i} - \epsilon_{S,j})](\hat{S}_i - \hat{S}_j) \frac{\partial(\hat{S}_i - \hat{S}_j)}{\partial \mathcal{P}}$. Thus, the gradient of Eq. 9 can be deemed as the gradient of Eq. 11 add some random noise scaled by $(\hat{S}_i - \hat{S}_j) \frac{\partial(\hat{S}_i - \hat{S}_j)}{\partial \mathcal{P}}$ for each sample. Let \hat{S}^\dagger denote the optimal solution of Eq. 11. Thus, $\mathcal{L}'_b(\hat{S}) \geq \mathcal{L}'_b(\hat{S}^\dagger), \forall \hat{S}$, and it satisfies Assumption 5.1 in (Bu et al., 2024).

$$\mathbf{g} = -\frac{1}{|\mathcal{B}|} \sum_{(i,j) \in \{(r,t) | r \in \mathcal{B}, t \in \mathcal{B}\}} \lambda_1(\epsilon_{s,i} - \epsilon_{s,j} + y_i - y_j)(\hat{S}_i - \hat{S}_j) \frac{\partial(\hat{S}_i - \hat{S}_j)}{\partial \mathcal{P}} + \lambda_2(\epsilon_{S,i} - \epsilon_{S,j} + y_i - y_j)(\hat{S}_i - \hat{S}_j) \frac{\partial(\hat{S}_i - \hat{S}_j)}{\partial \mathcal{P}} \quad (17)$$

$$\mathbf{g}' = -\frac{1}{|\mathcal{B}|} \sum_{(i,j) \in \{(r,t) | r \in \mathcal{B}, t \in \mathcal{B}\}} \lambda_1(y_i - y_j)(\hat{S}_i - \hat{S}_j) \frac{\partial(\hat{S}_i - \hat{S}_j)}{\partial \mathcal{P}} + \lambda_2(y_i - y_j)(\hat{S}_i - \hat{S}_j) \frac{\partial(\hat{S}_i - \hat{S}_j)}{\partial \mathcal{P}} \quad (18)$$

Since $y \in [0, 1], \hat{S} \in [0, 1], |y_i - y_j| \leq 1, \forall(i, j)$ and $|\hat{S}_i - \hat{S}_j| \leq 1, \forall(i, j)$. Thus, $|\mathbf{g}'_{i,j}| = |(y_i - y_j)(\hat{S}_i - \hat{S}_j) \frac{\partial(\hat{S}_i - \hat{S}_j)}{\partial \mathcal{P}}| \leq |\frac{\partial(\hat{S}_i - \hat{S}_j)}{\partial \mathcal{P}}|$. Furthermore, according to Appendix. A.9, conditional network is a multi-layer perceptron with sigmoid as its activation function. Let $\sigma(x)$ denote sigmoid function. Since $\sigma(x)' = \sigma(x)(1 - \sigma(x))$ and $0 < \sigma(x) < 1, |\frac{\partial(\hat{S})}{\partial \mathcal{P}}| < 1$. Thus, $|\frac{\partial(\hat{S}_i - \hat{S}_j)}{\partial \mathcal{P}}| \leq 1$. Thus, $|\mathbf{g}'_{i,j}| \leq 1$. Thus, $|\mathbf{g}'| \leq \frac{1}{|\mathcal{B}|} \sum_{i,j} |\mathbf{g}'_{i,j}| = 1$ Since \mathcal{L}'_b is L -Lipschitz continuous, $|\mathcal{L}'_b(\mathcal{P}_1) - (\mathcal{L}'_b(\mathcal{P}_2) + \mathbf{g}'^T(\mathcal{P}_1 - \mathcal{P}_2))| = |[\mathcal{L}'_b(\mathcal{P}_1) - \mathcal{L}'_b(\mathcal{P}_2)] + \mathbf{g}'^T(\mathcal{P}_1 - \mathcal{P}_2)| \leq L|\mathcal{P}_1 - \mathcal{P}_2| + |\mathbf{g}'_{i,j}| \cdot |\mathcal{P}_1 - \mathcal{P}_2| \leq (L + 1) \cdot |\mathcal{P}_1 - \mathcal{P}_2|$. Since $L \geq 0, L + 1 > 0$, it satisfies Assumption 5.2 in (Bu et al., 2024).

Since $\mathbb{E}(\mathbf{g}'_{i,j} - \mathbf{g}_{i,j}) = \mathbb{E}[(\lambda_1(\epsilon_{s,i} - \epsilon_{s,j}) + \lambda_2(\epsilon_{S,i} - \epsilon_{S,j}))(\hat{S}_i - \hat{S}_j) \frac{\partial(\hat{S}_i - \hat{S}_j)}{\partial \mathcal{P}}] = \mathbb{E}[(\lambda_1(\epsilon_{s,i} - \epsilon_{s,j}) + \lambda_2(\epsilon_{S,i} - \epsilon_{S,j}))](\hat{S}_i - \hat{S}_j) \frac{\partial(\hat{S}_i - \hat{S}_j)}{\partial \mathcal{P}}$. Since $\mathbb{E}(\epsilon_{s,i}) = \mathbb{E}(\epsilon_{s,j}), \mathbb{E}(\epsilon_{S,i}) = \mathbb{E}(\epsilon_{S,j}), \mathbb{E}[\lambda_1(\epsilon_{s,i} - \epsilon_{s,j}) + \lambda_2(\epsilon_{S,i} - \epsilon_{S,j})] = 0$. Thus, $\mathbb{E}(\mathbf{g}'_{i,j} - \mathbf{g}_{i,j}) = 0$. $\mathbb{E}|\mathbf{g}'_{i,j} - \mathbf{g}_{i,j}|^2 = (\hat{S}_i - \hat{S}_j)^2 (\frac{\partial(\hat{S}_i - \hat{S}_j)}{\partial \mathcal{P}})^2 \mathbb{E}[(\lambda_1(\epsilon_{s,i} - \epsilon_{s,j}) + \lambda_2(\epsilon_{S,i} - \epsilon_{S,j}))^2]$. As proven above, $|\hat{S}_i - \hat{S}_j| \leq 1$, thus $(\hat{S}_i - \hat{S}_j)^2 \leq 1$. Since $\frac{\partial(\hat{S}_i - \hat{S}_j)}{\partial \mathcal{P}} \leq 1, (\frac{\partial(\hat{S}_i - \hat{S}_j)}{\partial \mathcal{P}})^2 \leq 1$. Thus, $(\hat{S}_i - \hat{S}_j)^2 (\frac{\partial(\hat{S}_i - \hat{S}_j)}{\partial \mathcal{P}})^2 \mathbb{E}[(\lambda_1(\epsilon_{s,i} - \epsilon_{s,j}) + \lambda_2(\epsilon_{S,i} - \epsilon_{S,j}))^2] \leq \mathbb{E}[(\lambda_1(\epsilon_{s,i} - \epsilon_{s,j}) + \lambda_2(\epsilon_{S,i} - \epsilon_{S,j}))^2]$. Since $\epsilon_{s,i} \sim \mathcal{D}(\mu_s, \sigma_s), \epsilon_{s,j} \sim \mathcal{D}(\mu_s, \sigma_s)$ independently, $\mathbb{E}[(\epsilon_{s,i} - \epsilon_{s,j})^2] = 2\sigma_s^2$. Similarly, $\mathbb{E}[(\epsilon_{S,i} - \epsilon_{S,j})^2] = 2\sigma_S^2$. After simplifying its formation, we obtain $\mathbb{E}[(\lambda_1(\epsilon_{s,i} - \epsilon_{s,j}) + \lambda_2(\epsilon_{S,i} - \epsilon_{S,j}))^2] = 2\lambda_1^2\sigma_s^2 + 2\lambda_2^2\sigma_S^2$. Thus, $\mathbb{E}|\mathbf{g}'_{i,j} - \mathbf{g}_{i,j}|^2 \leq 2\lambda_1^2\sigma_s^2 + 2\lambda_2^2\sigma_S^2$. Then, it satisfies Assumption 5.3 in (Bu et al., 2024).

Therefore, \mathcal{L}'_b satisfies Assumption 5.1-Assumption 5.3 in (Bu et al., 2024). As proven before, minimizing \mathcal{L}_b by stochastic gradient descent can be deemed as adding a random noise to the gradient of each sample during the stochastic gradient descent process of \mathcal{L}'_b . Since Assumption 5.1-Assumption 5.3 in (Bu et al., 2024) hold, we can use Theorem 4 in (Bu et al., 2024) to prove that after adding these random noise, \mathcal{L}_b can also converge as quickly as \mathcal{L}'_b by $\mathbf{O}(T^{-\frac{1}{4}})$.

A.4. Proof of Theorem 3

Since when Assumption 1 - Assumption 4 hold, Lemma 1 is valid. Thus, using stochastic gradient descent (SGD) to minimize \mathcal{L}_b can be approximate to using stochastic gradient descent to minimize \mathcal{L}'_b , when iteration step approach infinity. Thus, we prove that optimal solution of \mathcal{L}'_b has the mentioned properties.

Proof of property 2. Let \hat{S}^\dagger denote the optimal solution of \mathcal{L}'_b . We use the proof of contradiction to prove it. We firstly assume if there are $r, k, r', k' \in [1, n]$ that satisfies Eq. 19-Eq. 20. By enlarging \hat{S}_r^\dagger by Δt and reducing $\hat{S}_{r'}^\dagger$ by Δt , we can further

decrease the value of \mathcal{L}'_b , which is contradict to the assumption that \hat{S}^\dagger is optimal. Thus, $\forall r, k, r', k'$, if $y_r - y_k > y_{r'} - y_{k'}$, then $\hat{S}_r^\dagger - \hat{S}_k^\dagger > \hat{S}_{r'}^\dagger - \hat{S}_{k'}^\dagger$.

Here is the detailed derivation. Without loss of generality, we can assume $y_r > y_{r'}$, because if $y_r < y_{r'}$, given $y_r - y_k < y_{r'} - y_{k'}$, $y_k < y_{k'}$. In this case, by multiplying minus one to both side of the inequality Eq. 19-Eq. 20, we can obtain a set of inequality that $y_{k'} - y_{r'} > y_k - y_r$, $\hat{S}_{k'}^\dagger - \hat{S}_{r'}^\dagger < \hat{S}_k^\dagger - \hat{S}_r^\dagger$ with the condition $y_{k'} > y_k$, which is equal to assuming $y_r > y_{r'}$ for Eq. 19-Eq. 20.

$$y_r - y_k > y_{r'} - y_{k'} \tag{19}$$

$$\hat{S}_r^\dagger - \hat{S}_k^\dagger < \hat{S}_{r'}^\dagger - \hat{S}_{k'}^\dagger \tag{20}$$

Let \hat{S}_r^\dagger grows to $\hat{S}_r^\dagger + \Delta t$ and $\hat{S}_{r'}^\dagger$ decreases to $\hat{S}_{r'}^\dagger - \Delta t$, where $\Delta t > 0$. Let \mathcal{L}_1 denote the value of \mathcal{L}'_b before changing \hat{S}_r^\dagger and $\hat{S}_{r'}^\dagger$, and \mathcal{L}_2 denote the value of \mathcal{L}'_b after changing \hat{S}_r^\dagger and $\hat{S}_{r'}^\dagger$. We compute the difference between \mathcal{L}_2 and \mathcal{L}_1 in Eq. 21. Furthermore, we can simplify it to Eq. 22. Given $y_r > y_{r'}$, $\mathcal{L}_1 - \mathcal{L}_2 > 0$, which means \mathcal{L}_2 is smaller than \mathcal{L}_1 . However, since \hat{S}^\dagger is the optimal solution of \mathcal{L}'_b , there should be no value set of \hat{S} that can make \mathcal{L}'_b smaller than \mathcal{L}_1 . Thus, the conclusion $\mathcal{L}_2 < \mathcal{L}_1$ is contradict to the assumption that \hat{S}^\dagger is optimal. Thus, $\forall r, k, r', k'$, if $y_r - y_k > y_{r'} - y_{k'}$, then $\hat{S}_r^\dagger - \hat{S}_k^\dagger > \hat{S}_{r'}^\dagger - \hat{S}_{k'}^\dagger$.

$$\begin{aligned} \mathcal{L}_1 - \mathcal{L}_2 = & \sum_{i=1, i \neq r}^n (y_i - y_{r'})\Delta t + \sum_{j=1, j \neq r}^n (y_{r'} - y_j)(-\Delta t) + (y_r - y_{r'})(2\Delta t) + (y_{r'} - y_r)(-2\Delta t) \\ & + \sum_{i=1, i \neq r'}^n (y_i - y_r)(-\Delta t) + \sum_{j=1, j \neq r'}^n (y_r - y_j)(\Delta t) \end{aligned} \tag{21}$$

$$\mathcal{L}_1 - \mathcal{L}_2 = 2n\Delta t(y_r - y_{r'}) \tag{22}$$

Proof of Property 1. Let $k = k'$. Then, according to property 2, $\forall r, k, r'$, if $y_r - y_k > y_{r'} - y_k$, $\hat{S}_r^\dagger - \hat{S}_k^\dagger > \hat{S}_{r'}^\dagger - \hat{S}_k^\dagger$. The inequality mentioned above can further reduced to $\forall r, r'$, if $y_r > y_{r'}$, $\hat{S}_r^\dagger > \hat{S}_{r'}^\dagger$.

A.5. Prompt Design

For each dataset, their prompts contain four parts: the expertise supplement, the input data, the task description and examples, where examples are chosen by the standard illustrated in set-up-pitch prompt. We list the concrete prompts for different datasets below. Since the prompt of aircraft monitoring datasets (Flight 1 and Flight 2) refers to trade secrets of the airline company, we do not list them below. Due to the randomness of LLM, we run multiple times and pick the one with best performance to collaborate with task-specific small model.

Prompt of MGAB

Input data description: The input data is a 10000 * 1 time series. The time series is generated by adding the value x , which satisfied $\frac{dx}{dt} = 0.25 * \frac{x(t-18)}{1+x(t-18)^{10}} - 0.1 * x(t)$, and some noises within range of $[-0.01, 0.01]$, where $x(t)$ represents the value of time series at t^{th} time slot. There are some anomalies inserted into the time series, which do not obey mentioned rules. The anomalies are inserted by repeating some future segment of the time series to present position.

Input data: {data}

Task description: Given the input data, please pick out the anomalies along the time series and output the possibility that the i^{th} time slot is anomalous. Please only output the corresponding possibility within the range of $[0, 1]$. (i is an iterable index).

Examples:

Example 1: Given the input data, please pick out the anomalies along the time series and output the possibility that the i^{th} time slot is anomalous. Please only output the corresponding possibility within the range of $[0, 1]$. Output: 0.

Example 2: Given the input data, please pick out the anomalies along the time series and output the possibility that the i^{th} time slot is anomalous. Please only output the corresponding possibility within the range of $[0, 1]$. Output: 1.

Prompt of Mustang

Expertise Supplement: The input data is a matrix with size $T * 17$, which represents the task duration time distribution for T time slots in cloud center. For each time slot, there are 17 dimensions. The values for these dimensions respectively represent the ratio of tasks whose duration time belongs to $[0,5)$, $[5,10)$, $[10, 20)$, $[20,30)$, $[30, 40)$, $[40, 70)$, $[70, 110)$, $[110, 150)$, $[150, 190)$, $[190, 230)$, $[230, 280)$, $[280, 330)$, $[330, 380)$, $[380, 430)$, $[430, 900)$, $[900, 1200)$, $[1200, 1900)$.

Input data: $\{data\}$.

Task description: Given a sliding window with size $50 * 17$, please judge if there are many tasks slowdown at a specific time slot, compared with other slots in given window. Please output a float number ranging from 0 to 1 to represent the probability that there are many tasks slowdown at the specific time slot.

Examples:

Example 1: Given the input data, please judge if there are many tasks slow down at time slot i and output a float number ranging from 0 to 1 to represent the probability of it. Response: 0.

Example 2: Given the input data, please judge if there are many tasks slow down at time slot i and output a float number ranging from 0 to 1 to represent the probability of it. Response: 1

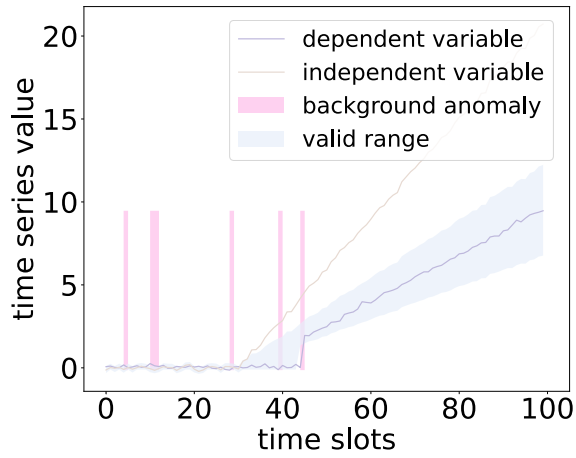
A.6. Anomaly classification

We use different binary classification standard to classify the anomalies in Flight 1 and Flight 2. Among them, the most common binary classification standard is point anomaly and contextual anomaly, which is illustrated in (Lai et al., 2024). Besides, we also introduce other two kinds of binary classification standard for aircraft monitoring dataset to explore the compensative effect between LLM and task-specific small model. According to the degree of reliance on expert knowledge for anomaly detection, we can divide anomalies into background anomaly and data pattern anomaly. The background anomalies highly rely on expertise knowledge, while the data pattern anomaly can be identified only by task-specific small model. As shown in Fig. 6(a), the valid range of dependent variable is decided by the independent variable, which should satisfy the laws of physics between different parameters. It is usually hard for neural network to clearly identify the valid range of the dependent variable, given independent variable. Thus, in this case, it rely on expertise knowledge and belongs to background anomaly. In contrast, in Fig. 1(a), the redundant channel mechanism usually requires most of redundant channel can reach a consensus. Thus, different redundant channels should always be similar to each other in normal status. In this situation, the neural network can identify the similarity between different channels without expertise knowledge. Thus, it belongs to data pattern anomaly. According to the similarity between anomaly and surrounding time series, we can divide anomalies into gradual anomalies and mutant anomalies. As shown in Fig. 6(c), the anomalies are quite different from surrounding normal time series and they should belong to mutant anomalies. In Fig. 6(d), the anomalies are similar to surrounding normal time series and they should belong to gradual anomaly.

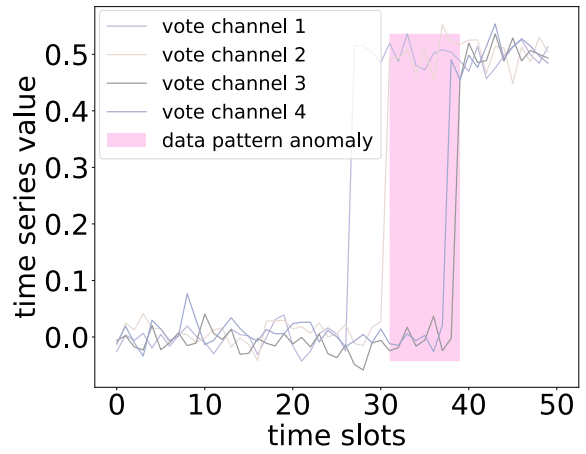
A.7. Datasets

In our experiments, we used four datasets from different scenarios: the cloud service monitoring, the aircraft monitoring, the mathematical-assumption-based anomaly datasets. We introduce these datasets in the following.

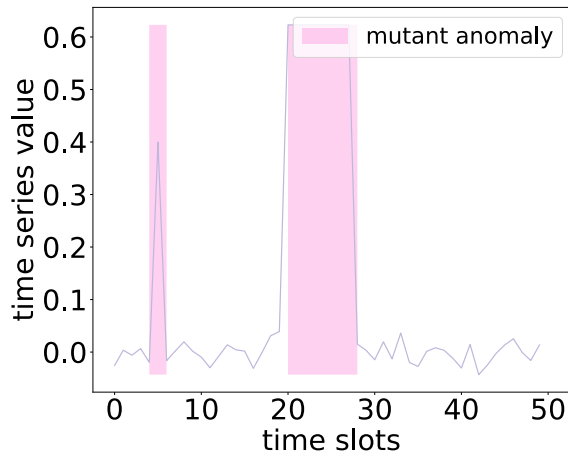
- **MGAB.** The dataset comprises synthetic Mackey-Glass time series characterized by non-trivial anomalies. Mackey-Glass time series are recognized for their propensity to exhibit chaotic behavior under specific conditions. The MGAB dataset encompasses 10 Megabytes (MG) of time series data, with each series extending to a length of 105 time points. Within each time series, 10 anomalies are meticulously introduced using a procedure outlined subsequently. Unlike other synthetic benchmarks, it poses a considerable challenge for the human eye to discern the artificially introduced anomalies from the inherent chaotic behavior. A segment of a time series featuring 3 anomalies is illustrated in the graph above. Due to the limit of computation resource when using LLM, we only use 10000 time slots in our experiments. Since there is no point anomalies in original dataset, but our model utilize the compensative effect of LLM and task-specific model on point anomaly and contextual anomaly, we insert some point anomalies into the



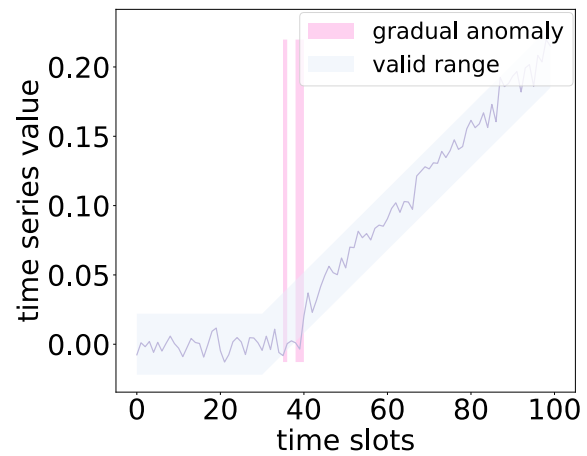
(a) The background anomaly



(b) The data pattern anomaly



(c) The mutant anomaly



(d) The gradual anomaly

Figure 6. These figures show different anomaly types

original dataset and release it in

- **Mustang.** The Mustang dataset chronicles the task duration of operations over a span of five years. The authors in (Chen et al., 2024b) have conducted preprocessing on the raw dataset, where they count the histogram of the task duration time distribution at each time slot. Subsequently they manually identified and labeled the slowdown anomalies. Due to the cost of LLM, we only use part of this dataset.
- **Flight 1 & 2.** These datasets are collected from a airline company, which is one of world top 150 enterprises. Different datasets contain monitoring data of different parameters of flight control system. The datasets use redundant channels (Osder, 1999) to ensure the robustness of flight system and refer to sophisticated collaborative relationship between different parameters, which introduces complex rules to judge the availability of the flight control system and is hard to be learned only by neural network. Besides, we show the ratios of normality and different kinds of anomaly in Fig. 7, where the anomaly classification is defined in Appendix. A.6.

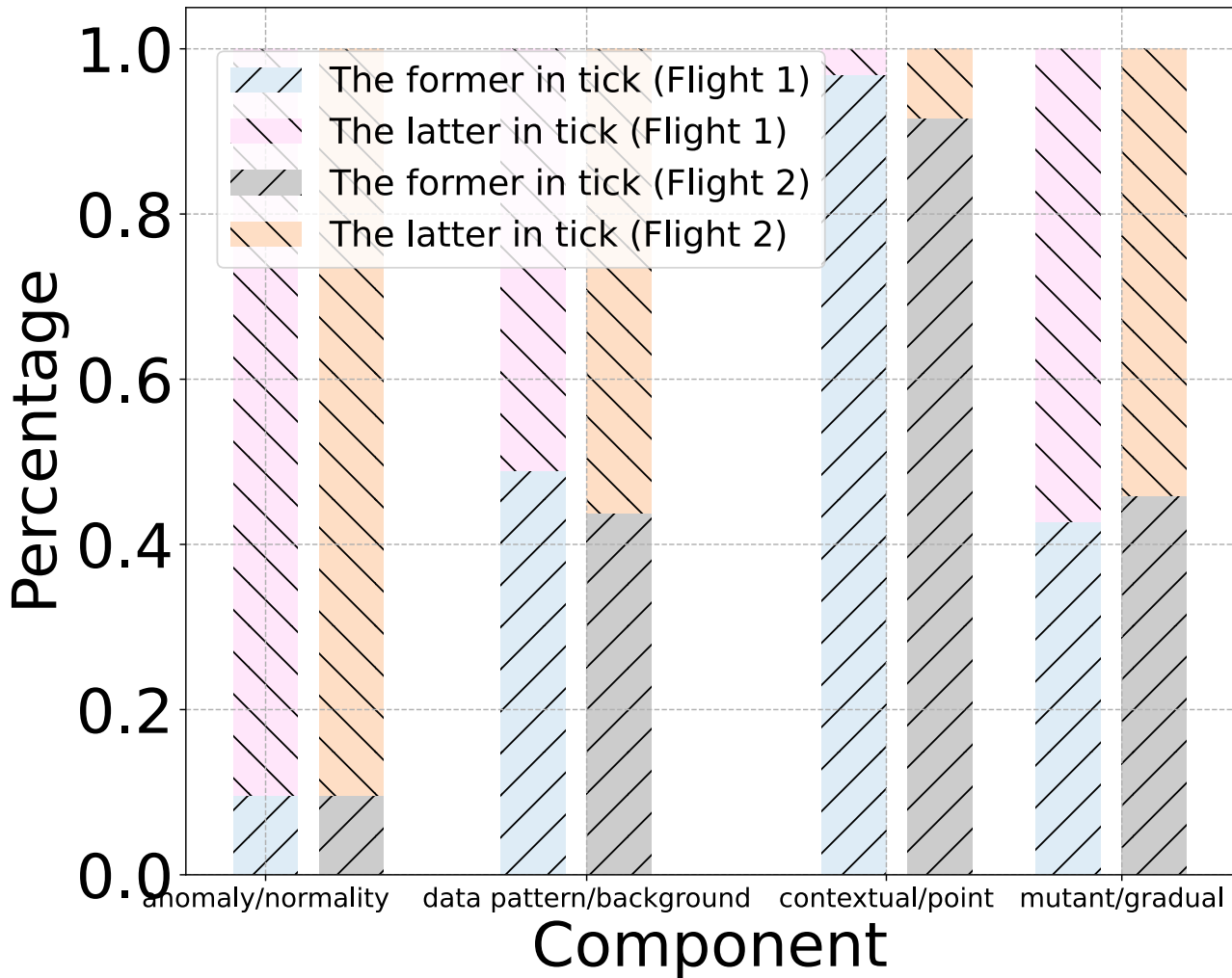


Figure 7. The distribution of Flight datasets

A.8. Hyperparameters

We illustrate the meaning of each hyperparameter in Tab. 3 and list the value of hyperparameter in Tab. 4. Since the datasets used in our experiments consist of several subsets. In some dataset, we set different hyperparameter values for different subsets and we list the values used in the Tab. 4. In these situations, we use grid search to find the optimal combinations of these hyperparameters for each subset.

Table 3. The meaning of each hyperparameter.

Hyperparameter Name	Meaning
winLen	The length of sliding window
moduleNum	The number of small model attention layers
batchSize	The size of batch
trlr	The learning rate of small model
colr	The learning rate during collaboration
patchSize	The size of patch in computin D_{inter} and D_{intra}
kLen	The length of convolution kernel in small model
d	The square root in Eq. 4
$\hat{\lambda}$	The weight of lagrange coefficient in \mathcal{L}_a

Table 4. The value of each hyperparameter.

Mustang		MGAB		Fligh 1		Flight 2	
Name	Value	Name	Value	Name	Value	Name	Value
winLen	4	winLen	5	winLen	2	winLen	2
moduleNum	6	moduleNum	10	moduleNum	6	moduleNum	10
batchSize	100	batchSize	100	batchSize	100	batchSize	100
trlr	0.001	trlr	0.01	trlr	0.01	trlr	0.01
colr	0.001,0.0001	colr	0.01 & 0.001	colr	0.008	colr	0.01,0.001
patchSize	2	patchSize	2	patchSize	2	patchSize	2
kLen	2	kLen	2	kLen	2	kLen	2
d	0.7,1.2	d	0,0.5,0.7,1,1.5	d	0,1.7,2	d	0.01,0.5,0.9,1.7,2
$\hat{\lambda}$	0.1,1	$\hat{\lambda}$	1	$\hat{\lambda}$	1,2,5	$\hat{\lambda}$	1,5

A.9. Architecture of conditional network

The conditional network uses the data representation obtained from task-specific small model as the condition and leverage the aligned anomaly score of small model and anomaly score of LLM to output collate anomaly score. As shown in Eq. 23, we firstly concat data representation, aligned anomaly score of small model and anomaly score of LLM as many conditional network do (Rakelly et al., 2018). After that, we use multilayer perceptrons to output collated anomaly score as shown in Eq. 24, where W_1 and W_2 are trainable parameters, σ_1 is leaky relu, and σ_2 is sigmoid function.

$$\bar{S} = \text{Concat}(S, s, R) \tag{23}$$

$$\hat{S} = \sigma_2(W_2\sigma_1(W_1 \cdot \bar{S})) \tag{24}$$